RSC Advances

ROYAL SOCIETY OF CHEMISTRY

www.rsc.org/advances

Cite this: DOI: 10.1039/c0xx00000x

www.rsc.org/xxxxxx

ARTICLE TYPE

Enhanced Photocatalytic activity of Nanocrystalline N - doped $ZnSb_2O_6$: role of N doping, cation ordering, particle size and crystallinity[+]

Nagarajan Arunkumar [a] and Rajagopalan Vijayaraghavan* [a]

Received (in XXX, XXX) Xth XXXXXXXXX 20XX, Accepted Xth XXXXXXXXX 20XX

DOI: 10.1039/b000000x

[+] One of the authors (R.V) dedicates this article to Professor C.N.R Rao FRS in Honour of his 80th Birthday.

Trirutile antimonate N - doped nanocrystalline $ZnSb_2O_6$ has been synthesised by a facile solution combustion method for the first time. The as synthesized products obtained with different oxidant to fuel ratios (O/F) itself are crystalline single phasic N - doped $ZnSb_2O_6$ as confirmed by powder X-ray diffraction (XRD). The products have been characterized well by Scanning Electron Microscopy (SEM), Energy Dispersive X-ray Analysis (EDAX), Transmission Electron Microscopy (TEM), Fourier - Transform Infrared Spectroscopy (FTIR) and X-ray Photoelectron Spectroscopy (XPS). Raman spectral modes of all the products show characteristic features of trirutile structure with shifting and broadening of spectral peaks in nanocrystalline products compared to that of microcrystalline product. UV-visible Diffused Reflectance Spectra (DRS) spectra confirm the decrease of band gap with increase in O/F and is in the range of 3.20 - 2.82 eV. Micro and nanocrystalline N - doped $ZnSb_2O_6$ show significant photocatalytic activity for degradation of Rhodamine (RhB). Furthermore, production of $^{\bullet}OH$ hydroxyl radicals was monitored through photoluminescence study by trapping $^{\bullet}OH$ radicals generated in the reaction mixture with terephthalic acid. The activity is found to correlate with the concentration of $^{\bullet}OH$ radicals and is found to be maximum for nanocrystalline ordered N-doped $ZnSb_2O_6$ which exhibits the highest activity indicated by its degradation efficiency and rate constant. The enhanced photocatalytic activity of combustion synthesized nanocrystalline N - doped $ZnSb_2O_6$ is reported for the first time here and the activity is found to correlate with N-doping, cation ordering, particle size and crystallinity.

Introduction

Oxide semiconductor materials act as photocatalysts for the light-induced photochemical reactions because of its unique electronic structure characterized by a filled valence band (VB) and an empty conduction band (CB) separated by an appropriate band gap[1]. Oxides, sulphides and nitrides of metals are potential semiconductor materials researched for photocatalytic splitting of water and dye degradation. Some transition metal oxides such as NiO, RuO_2 and oxides of noble metals (Pt, Rh, Au) function as co-catalysts for H_2 evolution in water splitting.[2,3] Photocatalytic degradation of organic compounds by semiconductor materials for the purpose of treatment of dye wastewater from industries is of much practical importance. In this process, the semiconductor photocatalysts oxidize the organic pollutants eventually to simple, non-toxic inorganics such as Cl^-, SO_4^{2-}, NO_3^-, CO_2 and H_2O through photocatalysis.[4] Antimonates of general formula, MSb_2O_6 (M = Zn, Mg, Co, Cd, Ca, Sr, Ba, Pb) are a class of inorganic photocatalyst extensively studied for this purpose. [3,5] These have also been studied for interesting transport properties, light emitting diodes and photovoltaic device applications in addition to photocatalysis.[3,5-13] In particular, $ZnSb_2O_6$ which is mineralogically known as ordenezite and crystallizes in trirutile-type structure, with the space group $P4_1/mnm$. Its structure is built up from two edge-sharing SbO_6 octahedra along c axis, sharing their corners with two other SbO_6 octahedra, M atoms are octahedrally coordinated by six O atoms in each rutile unit.[6,14] The features are (1) Dominant Sb 5s orbitals at the bottom of conduction band (2) Edge-shared MO_6 octahedron (M metal) aligned regularly in the trirutile-type structure.[15] Few Sb^{5+} based oxides in addition to $ZnSb_2O_6$, $BiSbO_4$,[16] $M_2Sb_2O_7$ (M = Ca, Sr)[17] all these antimonates based photocatalysts contain distorted Sb – O polyhedra which is attributed for its photocatalytic activity.[8] Nanocrystalline photocatalysts exhibit enhanced photocatalytic activity.[1,5] Therefore, considerable interest has been shown for the synthesis of zinc antimonates in nanocrystalline form and there are only few such reports, mostly on hydrothermal synthesis. [7,8,9] There is no report on combustion synthesis of $ZnSb_2O_6$ due to the fact that $SbCl_3$ (commonly

available salt of Sb) is not suitable for combustion synthesis, being a chloride salt. We circumvented this problem by addition of NH_4NO_3 along with the reactants which converts the chloride to NH_4Cl that sublimes off during combustion. Indeed, we are successful in synthesizing antimonates through combustion synthesis.

In the present work, we report the one pot synthesis of single phasic nanocrystalline N - doped $ZnSb_2O_6$ by urea assisted solution combustion method for the first time. The combustion of (Oxidant) metal nitrates – (Fuel) urea mixtures occurs as self-propagating and non-explosive exothermic reaction releasing heat along with evolution of large amounts of gases and intense flame. The powders synthesized with varying O/F ratio have been characterized. The advantage of this method is that the as synthesized products itself are crystalline without the need for further calcination. Cationic structural ordering and photocatalytic activity of microcrystalline $ZnSb_2O_6$ and nanocrystalline $ZnSb_2O_6$ have been investigated systematically. Significant photocatalytic activity has been observed for the degradation of aqueous Rhodamine B (RhB) solution under UV − light irradiation. Among all dyes, RhB is one of the most important representative of xanthenes based dye, an organic pollutant. It is widely used as a photosensitizer and can result in potentially carcinogenic aromatic amines.[18,19,20] Therefore, it is important to investigate its degradation to evaluate the activity of a photocatalyst.

Experimental

Materials and Reagents

The starting materials for the synthesis of $ZnSb_2O_6$ were $Zn(NO_3)_2.6H_2O$ 99.9 % (Sigma Aldrich), $SbCl_3$ 99.99% (Sigma Aldrich), NH_4NO_3 99.5% (S.D Fine chemicals, India) and NH_2CONH_2 99.5% (Thomas beaker, India). Sb_2O_3 99.99% (Sigma Aldrich) and ZnO 99.99% (Sigma Aldrich).

Preparation of microcrystalline $ZnSb_2O_6$ by solid state synthesis

Microcrystalline $ZnSb_2O_6$ was prepared by standard solid state method. Stoichiometric quantities of ZnO and Sb_2O_3 were mixed thoroughly. This mixture was heated at 600°C for 12h and finally at 900°C for 6h with intermediate grindings in a programmable thermolyne furnace (Model No: F46110CM-33) with a heating rate of 4°C / min and furnace cooled.

Preparation of Nanocrystalline N - doped $ZnSb_2O_6$ by combustion synthesis

Stoichiometric quantity of zinc nitrate is dissolved in minimum amount of deionised water. $SbCl_3$ mixed with NH_4NO_3 in 1:3 ratio is then added to the above metal nitrate solution followed by addition of fuel (urea). The solution was stirred thoroughly for 30 min for homogeneous mixing. This solution mixture was introduced into a preheated furnace kept at 400° C. The volume of solution gets reduced immediately with boiling of solution and soon combustion takes place with intense flame along with evolution of gases yielding the products. The schematic representation of combustion process is shown in Fig.1. The Oxidant-to-Fuel (O/F), one of the important parameter that plays a vital role on the combustion process[21, 22] and product formation is varied and three different (O/F) ratios for combustion were attempted, namely, 0.5, 1.0 and 2.0.

Characterization

The products were characterized by X-ray diffraction (XRD, Bruker D8 Advance with CuK_α radiation K_α λ = 1.5406 Å). Surface morphology and microstructure were examined by a Scanning Electron Microscope (FESEM Supra 55 - CARL ZEISS, Germany). Cationic ratio was analysed by EDS (Oxford Instruments, Liquid Nitrogen free SDD X MAX 50 EDS). Transmission Electron Microscope (TEM JEOL JEM 2100) was used for particle size measurement. The standard BET (Micromeritics ASAP 2020) method was employed for measurement of surface area. Fourier Transform Infrared (FT-IR) Spectrum was recorded over the range (400 – 3000 cm^{-1}) with (Shimadzu, IR Affinity-1S) spectrometer using KBr. X-Ray Photoelectron Spectra (XPS) were recorded using K-Alpha instrument (XPS K-Alpha surface analysis, Thermo fisher scientific, UK). All the binding energies were calibrated to C 1s internal standard peak (284.5 eV) and deconvolution of spectra was done using CASAXPS. Raman spectra were recorded on a laser Raman Spectrometer (Horiba Scientific/Lab RAM HR). Band analysis with a resolution in the order of 0.3 cm^{-1} to 1cm^{-1}. Optical absorption characteristics of the products were measured by UV − visible Diffused Reflectance Spectroscopy (DRS). Data were collected over the spectral range 200 - 1200 nm using (Jasco UV - Vis - NIR V- 670, Japan). Baseline spectra were collected using $BaSO_4$ as reference standard. Data were collected with a scan rate of 400 nm / min, at data interval of 1nm and signal UV/visible bandwidth of 5nm. Photocatalytic study was carried out at room temperature under UV light irradiation from six medium pressure mercury lamps 8W 254 nm UV lamps set in parallel to reaction tube. Heber multilamp photoreactor (model HML-MP-88) was used for photocatalysis. For estimation of photocatalytic activity, 50 mg of the photocatalyst was suspended in 50 ml of RhB (10 ppm) and this suspension was loaded in a photoreactor quartz tube. It was irradiated for different time durations using UV light. 2ml of aliquots were drawn from the reaction mixture at regular intervals (centrifuged to separate the photocatalyst) and the concentration of dye in the aliquots was continually monitored by measuring the absorbance at 554 nm, λ_{max} in a UV-Visible - spectrophotometer (Hitachi - 2910) to evaluate the photocatalytic activity. After completion of experiment, the photocatalyst was separated, dried at 100°C and used for the next cycle. Total organic carbon (TOC) was estimated using TOC analyzer (Elementar Vario TOC Select, Germany). Photocatalytic activity of semiconductor materials is largely attributed to reactive oxygen species especially, $^{\bullet}OH$ hydroxyl radicals from aqueous solutions under light. Hence, its measurement is important to understand the results of photocatalytic study. The production of $^{\bullet}OH$ radicals under UV irradiation was monitored by Photoluminescence (PL) technique (HITACHI (F-7000) Fluorescence Spectrophotometer) using terephthalic acid (TA) as the probe. TA readily reacts with $^{\bullet}OH$ hydroxyl radicals to generates 2-hydroxyterephthalic acid (TAOH) which emits fluorescence around 426 nm on excitation of its own 312 nm absorption band. The increase in photoluminescent intensity of TAOH with time should be directly proportional to the $^{\bullet}OH$ radicals generation. For this experiment,

50 mg of the photocatalyst was added to a 50 ml mixture of TA solution (3 mmol) and NaOH (10 mmol). From this mixture, 2 ml aliquots were sampled out at regular intervals after UV irradiation and the corresponding PL intensities were measured.

Results and Discussion

Structural Characterization

Powder XRD pattern Fig. 2(a) of $ZnSb_2O_6$ synthesized by solid state method confirms single phasic (JCPDS no. 38-0453) microcrystalline $ZnSb_2O_6$ ordered trirutile structure with characteristic reflections of (0 0 2), (1 0 1) and (1 1 2) having the lattice parameters of a = 4.6719 Å; c = 9.2646 Å with space group of $P4_2/mnm$. XRD patterns Fig. 2(b) of combustion synthesized products with different fuel ratios confirm that the as prepared products itself are crystalline single phase possessing disordered trirutile structure (absence of the above characteristic reflections). More importantly, all the diffraction lines show significant peak broadening indicating nanocrystalline nature of the as synthesized products crystallizing in tetragonal unit cell with parameters, a ~ 4.6692 Å, c ~ 3.0784 Å. No new diffraction peaks are observed for the N doped phases. In ordered trirutile structure, Zn^{2+} and Sb^{5+} are arranged in an 1:2 order along z-axis so that the "c" cell parameter is equal to three times that of disordered rutile structure, giving some characteristic reflections such as (0 0 2), (1 0 1), and (1 1 2) due to cationic ordering.[9,15] The structural disordering observed in as synthesized nanocrystalline N – doped $ZnSb_2O_6$ may be due to the low synthetic temperature employed as ordered trirutile structure is attained only at higher processing temperature. To improve the ordering network of nanocrystalline N-doped $ZnSb_2O_6$ and also to arrive at the disorder – order transition, the as synthesised nanocrystalline product obtained at O/F ratio of 1.0 was calcined at 500° C, 600 ° C, 700° C and at 900° C for 12h each. From ESI (Fig.S1 †) it is evident that at calcinations less than 700° C, no ordering was observed. Above 700° C ordering takes place as revealed by the appearance of characteristic reflections in the XRD patterns. In general, increase in the calcination temperature increases the crystallite size indicated by the decrease of peak broadening. The average crystallite sizes calculated from powder XRD pattern using the Scherrer's formula are given in ESI (Table S1 †)

Surface morphology

SEM images Fig.3 (a and c), of microcrystalline and nanocrystalline N-doped $ZnSb_2O_6$ (O/F = 1) reveal spherical shaped morphology of the products. EDAX patterns Fig. 3(b and d) confirms the cationic ratio to be equal to nominal compositions. TEM image Fig.4 (a) of as prepared N-doped $ZnSb_2O_6$ obtained with an O/F = 1 shows spherical shaped particles having average particle sizes of 10 − 20 nm with agglomeration and this is consistent with crystallite size calculated from XRD. The selected area electron diffraction pattern Fig.4 (b) reveals diffused continuous ring pattern confirming the formation of small polycrystalline grains. The BET surface area of microcrystalline $ZnSb_2O_6$ and nanocrystalline N - doped $ZnSb_2O_6$ (as prepared and calcined at 600° C, 700° C) are listed in ESI (Table S2†) indicating that combustion synthesized compounds are nanocrystalline with larger surface area.

FT-IR Spectra

FT-IR spectra of $ZnSb_2O_6$ and N-doped $ZnSb_2O_6$ obtained with O/F = 1 are shown in ESI (Fig.S2 a and b †). The absorption bands at 491, 493 cm^{-1} can be assigned to the symmetric deformation mode of Zn – O in ZnO_6 octahedra.[23] A strong band at 675, 680 cm^{-1} and then a weak band at 630, 636 cm^{-1} are assigned to O – Sb^{5+}– O in SbO_6 octahedra.[24] Bands at 586,795,798 cm^{-1} correspond to Sb^{5+}– O stretching vibrations.[25] N-doped $ZnSb_2O_6$ shows additional bands around 1402, 1285 and 1062 cm^{-1} attributed to vibrations of NO , NO_2^- like species bound to Zn, NH_3 like species bound to Zn and Zn – O – N respectively ESI (Table S3 †).

XPS Spectra

The XPS spectra Fig 5(a) of N-doped $ZnSb_2O_6$ (O/F = 1.0), exhibit peaks at binding energies of 395.3, 399.5 and 406.1 eV corresponding to N 1s with N in different chemical states. Based on literature, there could be four types of N species in N doped oxides, in the form of surface adsorbed NH_3 molecules, oxynitride in the form of O – Zn – N, N species bound to surface oxygen sites like NO, NO_2 and N^{3-} ion. Absence of peak at 397.6 eV rules out N^{3-} ion in our compositions. The peaks observed at 395.3, 399.5 and 406.1 eV confirm N in the form of NH_3 species,[26] oxynitride (O – Zn – N),[28] NO or NO_2 like species[27,29,30] respectively. The amount of nitrogen in N–$ZnSb_2O_6$ (O/F = 1.0) sample from XPS was found to be 4.5 atomic %. The O 1s region Fig 5(b) shows three peaks, 530.6 eV attributed to Zn − O lattice oxygen (O_L), 532.2 eV attributed to oxygen of surface hydroxyl OH group and 533.4 eV to adsorbed oxygen (O_{ad}).[31]

Raman Spectra

Trirutile structures belong to space group ($P4_2/mnm$). Raman spectra Fig.6 (a) of microcrystalline $ZnSb_2O_6$ exhibit bands in the range 200 to 800 cm^{-1} characteristic of trirutile structure indicating single phasic nature of the products. Raman bands in the range 800 – 600 cm^{-1} correspond to simple bridging bond vibration Sb − O_b − Sb, 600 – 500 cm^{-1} corresponds to Sb − O_{cyc} vibrations and Sb – Ob − Sb coupled with M^{2+} − O vibrations. 400 – 200 cm^{-1} due to M^{2+}– O vibrations.[24,33] All N-doped $ZnSb_2O_6$ products exhibit a similar spectra Fig.6 (b and c) as that of microcrystalline $ZnSb_2O_6$ but with peak broadening revealing that the particles are in nanocrystalline nature.[21] The systematic shifts in Raman bands could be attributed to different amounts of N - doping in the oxygen lattice effected by different amounts of the fuel.[27] Raman peaks are listed in ESI (Table S4 †).

Optical band gap

UV- vis diffuse reflectance spectra in the wavelength range 200 - 1200 nm are shown in Fig. 7(a). Reflectance increases with increasing fuel content. The reflectance was transformed to absorbance by using Kubelka – Munk conversion (1)

$$(\alpha/S) = (1-R)^2/2R \text{ ---------- (1)}$$

Where α is absorption coefficient, S is scattering coefficient and R is diffused reflectance at certain energy.[34,35] The absorption spectra Fig.7 (b) of microcrystalline $ZnSb_2O_6$ shows absorption edge at 370 nm whereas for N-doped $ZnSb_2O_6$ the absorption edge is in the range of 400 − 460 nm depending on the O/F ratio. At the same time a pronounced absorption tail is observed in the visible and near infrared regions for nanocrystalline N- doped $ZnSb_2O_6$. The possible reason might involve oxygen vacancies caused by different amounts of N-doping effected through varying fuel amounts employed in the combustion.[36-40] In micron sized $ZnSb_2O_6$, there is no absorption tail in the visible and infra red region indicating possibly the absence of oxygen vacancies. In these N-doped products, the absorption edge is also red shifted resulting in significant reduction in band gap compared to microcrystalline $ZnSb_2O_6$. The optical band gap is determined from absorption spectrum Fig. 7(c) using Tauc's relation, equation (2). [41, 42]

$$(\alpha h\upsilon)^n = A(h\upsilon - E_g) \quad \text{--------- (2)}$$

Where α denotes absorption coefficient, hν is the discrete photo energy, A is constant, E_g is the band gap and exponent n depends on type of transition, n = 2 for direct transition. Band gap of microcrystalline $ZnSb_2O_6$ is 3.35 eV and for nanocrystalline N - $ZnSb_2O_6$ it is in the range of 2.82 − 3.20 eV depending on the oxidant to fuel ratio. Band gap decreases significantly with increase in O/ F ratio and are listed in Table 1. The facile urea assisted combustion synthesis results in a reduction of 0.53 eV in the band gap of $ZnSb_2O_6$ due to N-doping in comparison to microcrystalline $ZnSb_2O_6$ and consequently a red-shift of the absorption edge by ~ 90 nm. The colours of the compounds obtained with varying fuel contents are consistent with the band gaps Table 1. N doping could lead to the formation of localized energy level / defects within the band gap closer to VB but on top of VB causing the reduction in band gap[3, 5, 43] Fig. 8 shows schematic band structure of $ZnSb_2O_6$ and N-doped $ZnSb_2O_6$.

In order to study the influence of cation ordering - disordering in trirutile structure on the band gaps, band gaps of disordered and ordered phases of N- $ZnSb_2O_6$ are calculated from Tauc's plot Fig. 7 (d). The disordered N-$ZnSb_2O_6$ (O/F = 1) phase is nanocrystalline and has a band gap of 2.9 eV. In order to increase the cation ordering, the disordered phase has been calcined at 700°C for12h (Fig S1). The resulting ordered, more crystalline N-$ZnSb_2O_6$ has a band gap of 3.2 eV. The latter exhibits a blue shift in the absorption edge in comparison to the former as revealed by UV-Vis DRS spectra and their colours. It indicates that calcination of the disordered N- $ZnSb_2O_6$ at 700°C may possibly eliminate N-doping leading to $ZnSb_2O_6$ with ordering that leads to increase in band gap and crystallinity in the latter.

Photocatalytic activity

$ZnSb_2O_6$ is a potential photoactive material for organic dye degradation[3,5,7,8]. For example, nanocrystalline $ZnSb_2O_6$ synthesized by hydrothermal method has been studied for degradation of Rhodamine (RhB) and Methylene Blue (MB).[7,8] We expect that nanocrystalline N - doped $ZnSb_2O_6$ will also be a good photocatalytic material under UV irradiation for dye degradation as the band gaps are in that range and hence evaluated the photocatalytic performance of micron sized ordered $ZnSb_2O_6$, nanocrystalline N - doped disordered $ZnSb_2O_6$ (O/F = 1, as prepared) and ordered trirutile nanocrystalline N - doped $ZnSb_2O_6$ (700° C calcined) by studying the degradation of typical zwitterionic dye (Rhododamine B - RhB), an organic pollutant, under UV light irradiation. Sequential changes in the concentration of RhB monitored by measuring the absorbance at the wavelength, 554 nm (λ_{max}), are shown in ESI (Fig. S3 a, b and c †).These compositions show negligible activity under visible light even after 2h irradiation. Photodegradation of RhB dye is visibly observed for all the compositions and the maximum absorbance λ_{max} at 554nm decreases, due to stepwise degradation of conjugated chromophore content in RhB during photocatalytic process.[44] The temporal changes Fig. 9(a) of RhB concentration during photodegradation are recorded as C/C_O, where C is concentration of RhB at particular irradiation time and C_O concentration at zero point time. Degradation efficiency is highest for ordered trirutile nanocrystalline N - doped $ZnSb_2O_6$ Fig.9 (b) and ESI (Table S5 †). Between the ordered and disordered phases of nanocrystalline N - doped $ZnSb_2O_6$, ordered phase exhibits better activity although it has a surface area (24.7 m^2 /g) lower than the disordered phase (35.2 m^2/g). It indicates that crystallinity is a prime material parameter for photocatalytic activity of a given material as high crystallinity in a photocatalyst decreases the defect density and disorder in materials.[2,45,46] The other parameters of importance for a photocatalyst are i) band structure ii) band gap iii) surface area. Crystallinity and ordering are directly related.

In order to compare the reaction kinetics of the photodegradation of RhB quantitatively, Langmuir-Hinshelwood (L-H) kinetics model was applied as per pseudo first-order equation (3) [47-50]

$$\ln (C/C_o) = - kt \quad \text{--------- (3)}$$

The kinetics of photocatalytic degradation for microcrystalline $ZnSb_2O_6$, nanocrystalline N – doped $ZnSb_2O_6$ and ordered N – doped $ZnSb_2O_6$ follow the expected first order as shown in ESI (Fig.S4 †) which presents a linear correlation ($R^2 > 0.97$) between ln (C/C_o) and irradiation time. Here, C represents the RhB concentration at time t, and C_o represents the initial RhB concentration and from the plot between ln (C/C_o) and irradiation time, the first-order rate constant k was determined and listed in ESI (Table S5†). The results indicate that ordered N – doped $ZnSb_2O_6$ exhibits fastest photocatalytic activity than disordered N – doped $ZnSb_2O_6$ and microcrystalline $ZnSb_2O_6$, the former having a rate constant more than three times that of the latter.

Mechanism of photocatalytic activity of N - doped $ZnSb_2O_6$

The band gaps of nanocrystalline disordered N - doped $ZnSb_2O_6$ and microcrystalline $ZnSb_2O_6$ are 2.9 and 3.35 eV respectively, so that these can be activated by UV light irradiation for generation of electron-hole pairs which are responsible for photocatalytic degradation of organic pollutants. Under the UV-light irradiation, in N - doped $ZnSb_2O_6$ electrons excited from the valence band (VB) to conduction band (CB) called the photogenerated electrons could react with the dissolved O_2 in the solution adsorbed on the surface of the photocatalyst to yield $^{\bullet}O_2^-$ superoxide anion radical.[50,51] While h^+ reacts with the OH^- to form $^{\bullet}OH$ hydroxyl radical. The dye molecules could be photodegraded via the reaction with $^{\bullet}O_2^-$ and $^{\bullet}OH$ radicals to form CO_2, H_2O and other mineral acids.[52,53] Possible photodegradation mechanism of N – doped $ZnSb_2O_6$ is shown Scheme [1], Fig. 10.

N - doped $ZnSb_2O_6$ + hν ⟶ $h^+_{VB} + e^-_{CB}$ ----- Scheme (1)

$h^+_{VB} + H_2O$ ⟶ $H^+ + {}^{\bullet}OH$

$e^-_{CB} + O_2$ ⟶ ${}^{\bullet}O_2^-$

RhB + ${}^{\bullet}O_2^- + {}^{\bullet}OH$ ⟶ $CO_2 + H_2O$ + Mineral acids

Determination of ${}^{\bullet}OH$ radical by Photoluminescence Spectra

Most of the photocatalytic dye degradation process involves the reaction of holes with surface adsorbed water and hydroxyl groups to produce reactive ${}^{\bullet}OH$, hydroxyl radicals which are mainly responsible for photodegradation. In order to estimate the rate of formation of active ${}^{\bullet}OH$ hydroxyl radicals under UV light irradiation, we employed terephthalic acid method in which terephthalic acid (TA) readily reacts with ${}^{\bullet}OH$ radicals to produce highly fluorescent 2-hydroxyterephthalic acid (TAOH), Fig.11(a) which emits fluorescence around 426 nm on excitation at 312 nm absorption band.[54-56] Hence, by monitoring the fluorescence intensity of TAOH with irradiation time, we can estimate the concentration of hydroxyl radicals. After UV irradiation, TA suspension along with photocatalyst (microcrystalline $ZnSb_2O_6$, nanocrystalline ordered and disordered N – doped $ZnSb_2O_6$) shows increase in PL intensity with time indicating increasing concentration of active ${}^{\bullet}OH$ radical species Fig.11 (b). It clearly confirms that the efficiency of degradation of $ZnSb_2O_6$ and N-doped $ZnSb_2O_6$ correlates with the amounts of active photogenerated ${}^{\bullet}OH$ hydroxyl radicals ESI (Table S5†) and it is the highest for ordered nanocrystalline phase which exhibits the maximum efficiency and fast kinetic for RhB degradation. The concentration of ${}^{\bullet}OH$ radicals linearly increases with increasing irradiation time ESI (Fig.S5 †) as expected and is maximum for nanocrystalline ordered $ZnSb_2O_6$.

Total organic carbon (TOC) measurements

TOC estimation for micro and nanocrystalline N - doped $ZnSb_2O_6$ photocatalyst is plotted in Fig.12 Decrease in TOC content with irradiation time reveals degradation (or) mineralization by the photocatalyst. Mineralization is more rapid for N-doped phases than for $ZnSb_2O_6$. RhB photodegradation occurs via two steps, first based on N-demethylation and then the breaking of conjugated chromophores in RhB. RhB is converted to smaller organic species and finally is mineralized to inorganic products such as CO_2 and H_2O. [44, 50]

Stability of photocatalyst

The stability of nanocrystalline ordered N-doped $ZnSb_2O_6$ photocatalyst was evaluated for four runs under the same experimental conditions. The catalyst did not exhibit any significant loss of activity between four cycles ESI (Fig. S6†) revealing the good stability of the photocatalyst and hence, could be recycled for photocatalytic degradation of dyes.

Conclusion

Our work illustrates the application of combustion synthesis for nanocrystalline antimonates in single phasic form in one step. Use of urea incorporates nitrogen into the oxygen lattice confirmed by FT-IR and XPS. Band gap value is tuned from 2.82 to 3.20 eV by varying the fuel ratios. Photocatalytic activity study indicates that nanocrystalline ordered N – doped $ZnSb_2O_6$ can effectively degrade RhB than disordered nanocrystalline and ordered microcrystalline phase. The former generates more amounts of hydroxyl radicals in aqueous solution in presence of UV light. This work demonstrates that nanocrystalline N - doped $ZnSb_2O_6$ phases perform as better photocatalysts than the well known photocatalyst $ZnSb_2O_6$ and are more promising materials for photocatalytic applications.

Acknowledgements

Authors thank VIT University for financial support and encouragement. Dr.V.Thangadurai, Department of Chemistry, University of Calgary, Canada is acknowledged for discussion.

Notes and references

[a] *Centre for Excellence in Nano Materials, Materials Chemistry Division, School of Advanced Sciences, VIT University, Vellore - 632 014, India. *Corresponding author: E-mail: rvijayaraghavan@vit.ac.in,* Tel: +91 0416 220 2460.

†Electronic Supplementary Information (ESI) available: See

DOI: 10.1039/b000000x/

1. H. Tong, S. Ouyang, Y. Bi, N. Umezawa, M. Oshikiri and J Ye, *Adv. Mater.,* 2012, **24,** 229–251.
2. A.Kudo and Y.Miseki,*Chem. Soc. Rev.,* 2009, **38**, 253-278.
3. S. Wu, G. Li, Y. Zhang and W. Zhang, *Mater. Res. Bull.*, 2013, **48**, 1117-1121.
4. J. Tang, Z. Zou and J. Ye, *Chem. Mater.,* 2004, **16**, 1644-1649.
5. D.P.Dutta, A. Ballal, A. Singh, M. H. Fulekar and A. K. Tyagi, *Dalton Trans.,* 2013, **42**, 16887-16897.
6. H. Mizoguchi and P. M. Woodward, *Chem. Mater.,* 2004, **16**, 5233 - 5248.
7. J. Singh, N. Bhardwaj and S.Uma, *Bull. Mater. Sci.,* 2013, **36**, 287-291.
8. W. Liu, P. Lin, H. Jin, H. Xue, Y. Zhang and Z. Li, *J.Mol. catal. A: chem.*, 2011, **349**, 80-85.
9. J. Jang and S.J Kim. *Jpn. J. Appl. Phys.,* 2012, **51**, 10NE23-1−10NE23-4.
10. X. Lin, J. Wu, X. Lu , Z. Shan, W. Wang and F. Huang, *Phys. Chem. Chem. Phys.,* 2009, **11**, 10047-10052.
11. M. Zhang, L. Chen, S. Yao, Y. Long, W. Li and Z. Wang, *Catal. Commun.,* 2014, **48**, 29-32.
12. A. Jamal, M.M. Rahman, S. B. Khan, M. Faisal , K. Akhtar, M. A. Rub, A. M. Asiri and A. O. Al-Youbi, *Appl.Surf. Sci.,* 2012, **261**, 52-58.
13. K. Zhang, X. Lin, F. Huang and W. Wang, *J.Mol. catal. A: chem.,* 2006, **258**, 185-190.
14. N. Kikuchi, H. Hosono and H. Kawazoe, *J. Am. Ceram. Soc.*, 2005, **88**, 2793-2797.
15. S. Matsushima, T.Tanizaki, H.Nakamura, M.Nonaka and M.Arai, *Chem.lett.,* 2001, **31**, 1010 - 1011.
16. Q. You, Y. Fu, Z. Ding, L. Wu, X. Wang and Z. Li, *Dalton Trans.,* 2011, **40**, 5774-5780.
17. X. Lin, F. Huang, W. Wang, Y. Wang, Y. Xia and J. Shi, *Appl. Catal. A.,* 2006, **313**, 218-223.
18. T.Fujii, H. Nishikiori and T. Tamura, *Chem. Phys. Lett.,* 1995, **233**, 424 - 429.
19. H. Fu, C. Pan, W. Yao and Y. Zhu, *J. Phys. Chem. B.,* 2005, **109**, 22432-22439.
20. S. Horikoshi, F. Hojo, H. Hikaka and N. Serpone, *Environ. Sci. Technol.,* 2004, **38**, 2198 - 2208.

21. K. Boobalan, R. Vijayaraghavan, K. Chidambaram, U. Kamachi Mudali and Baldev Raj, *J.Am.Ceram.Soc.,* 2010, **93**, 3651-3656.
22. K.C. Patil, *Bull. Mater. Sci.,* 1993, **16**, 533-541.
23. C. S. Lim, J. H. Ryu, J. G. Choi, C. Y. Park and W.C. Oh, *J. Ceram. Process. Res.,* 2011, **12**, 218-221.
24. S. Bahfenne and R.L. Frost, *Appl. Spectrosc. Rev.,* 2010, **45**, 101-129.
25. J. R. Reddy, G. Ravi, P. Suresh, N. K. Veldurthi, R. Velchuri and M. Vithal, *J. Therm. Anal. Calorim.,* 2014, **115**, 1321-1327.
26. H. Li, J.Li and Y. Huo, *J. Phys. Chem. B.,* 2006, **110**, 1559-1565.
27. G. Yang, Z. Jiang, H. Shi, T. Xiao and Z. Yan, *J. Mater. Chem.,* 2010, **20**, 5301-5309.
28. X. Zong, C. Sun, H. Yu, Z. G. Chen, Z. Xing, D. Ye, G. Qing (Max) Lu, X. Li and L. Wang, *J. Phys. Chem. C.,* 2013, **117**, 4937- 4942.
29. J. Ananpattarachai, P. Kajitvichyanukul and S.Seraphin, *J. Hazard.Mater.,* 2009, **168**, 253-261.
30. K.Toyoura, H. Tsujimura, T. Goto, K. Hachiya, R. Hagiwara and Y. Ito, *Thin Solid Films.,* 2005, **492**, 88-92.
31. N. P. Herring, L. S. Panchakarla and M. Samy El-Shall, *Langmuir.,* 2014, **30**, 2230−2240.
32. X. Xu, D. Chen, Z. Yi, M. Jiang, L. Wang, Z. Zhou, X. Fan,Y. Wang and D. Hui, *Langmuir.,* 2013, **29**, 5573-5580.
33. H. Haeuseler, *Spectrochim.Acta, Part A.,* 1981, **37**, 487-495.
34. P. Kubelka, and F.Z Munk, *Tech. Phys. (Leipzig).,*1931, **12**, 593.
35. W. C. Sheets, E.S. Stampler, M.I. Bertoni, M. Sasaki, T. J. Marks, T. O. Mason and K.R. Poeppelmeier, *Inorg. Chem.,* 2008, **47**, 2696 - 2705.
36. L. Xiao, S. Zhang and J. Huang, *Powder Technol.,* 2014, **258**, 297 - 303.
37. T .Nutz and M. Haase, *J. Phys. Chem. B.,* 2000, **104**, 8430-8437.
38. H. Irie, Y. Watanabe and K. Hashimoto, *J. Phys. Chem. B*., 2003, **107**, 5483-5486.
39. C. Burda, Y. Lou, X. Chen, A.C.S. Samia, J. Stout and J. L. Gole, *Nano Lett.,* 2003, **3**, 1049-1051.
40. X. Qiu and C. Burda, *Chem.Phys.,* 2007, **339**, 1–10.
41. J. Tauc, R. Grigorovici and A. Vancu, *Phys. Status Solidi B.,*1966, **15**, 627-637.
42. P.P. Sahoo and Paul A. Maggard, *Inorg. Chem.,* 2013, **52**, 4443 - 4450.
43. Z. Zou, J.Ye, K. Sayama and H. Arakawa, *Nature.,* 2001, **414**, 625 - 627.
44. C. Chen, W. Zhao, P. Lei, J. Zhao and N. Serpone, *Chem.Eur. J.,* 2004, **10**, 1956-1965.
45. F. Amano, A. Yamakata, K. Nogami, M. Osawa and B. Ohtani, *J. Am. Chem. Soc.*, 2008, **130**, 17650-17651.
46. W. Zhang, J. Tang and J. Ye, *J. Mater. Res.,* 2007, **22**, 1859-1871.
47. H. Huang, G.Chen and Y. Zhang, *Inorg. Chem. Commun.,* 2014, **44**, 46-49.
48. H. Huang, K. Liu, K. Chen, Y. Zhang, Y. Zhang and S. Wang, *J. Phys. Chem. C*., 2014, **118**, 14379-14387.
49. Y. Li, W. Wu, P. Dai, L. Zhang, Z. Sun, G. Li, M. Wu, X. Chenc and C. Chen, *RSC Adv.,* 2014, **4**, 23831-23837.
50. J. Luan, K. Ma, B. Pan, Y. Li, X. Wu and Z. Zou, *J.Mol.catal. A: chem.,* 2010, **321**, 1-9.
51. J. Liu, X. Pu, D. Zhang, H. Jin Seo, K. Du and P. Cai, *Mater. Res. Bull.,* 2014, **57**, 29-34.
52. Y. Chiang and C. Lin, *Powder Technol.,* 2013, **246**, 137-143.
53. S. Balachandran and M.Swaminathan, *J.Phys.Chem.C.,* 2012, **116**, 26306−26312.
54. T. Hirakawa and Y. Nosaka, *Langmuir.,* 2002, **18**, 3247- 3254.
55. Z. Chen, D. Li, W. Zhang, Y. Shao, T. Chen, M. Sun and X. Fu, *J. Phys. Chem. C.,* 2009, **113**, 4433-4440.
56. S. Uma, J. Singh, V. Thakral, *Inorg.Chem.,* 2009, **48**, 11624-11630.

Graphical Abstract

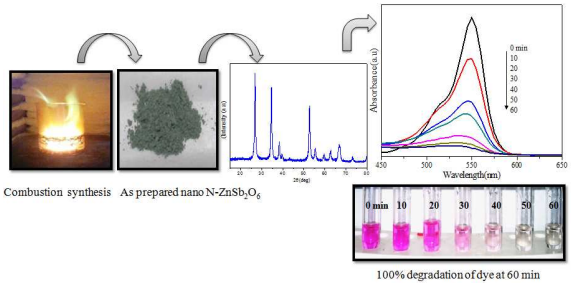

Textual Abstract

Nanocrystalline N - doped $ZnSb_2O_6$ is synthesized in a single step in single phasic form by a novel combustion method.

List of Figures

Fig.1 Schematic representation of combustion synthesis of N - doped $ZnSb_2O_6$

Fig.2 XRD patterns of (a) $ZnSb_2O_6$ (solid state synthesis) (b) nanocrystalline N- doped $ZnSb_2O_6$ with varying O/F ratio (combustion synthesis)

Fig.3 SEM and EDAX pattern of microcrystalline $ZnSb_2O_6$ (a & b) nanocrystalline N-doped $ZnSb_2O_6$ (c & d)

Fig.4 TEM image (a) and SAED pattern (b) of N-doped $ZnSb_2O_6$

Fig.5 XPS spectra of N - doped $ZnSb_2O_6$ (a) N1s spectrum (b) O1s spectrum

Fig.6 Raman spectra of (a) Microcrystalline $ZnSb_2O_6$ (b) Nanocrystalline N - doped $ZnSb_2O_6$ O/F = 0.5 and 1 (c) O/F = 2

Fig.7 (a) Diffused reflectance spectra (b) KM Absorbance spectra (c) Tauc's plot (d) Tauc's plot for ordered and disordered N - doped $ZnSb_2O_6$

Fig.8 Schematic band structures of $ZnSb_2O_6$ and N-doped $ZnSb_2O_6$.

Fig.9 (a) Temporal changes of RhB concentration as observed by UV-vis absorption spectra at λ_{max} 554nm; (b) Photodegradation of RhB with irradiation time.

Fig.10 Possible mechanism for photocatalytic degradation by $ZnSb_2O_6$

Fig.11 (a) Schematic reprentation of TAOH formation (b) Photoluminescence spectra of TAOH for ordered N-doped $ZnSb_2O_6$

Fig.12 Total Organic Carbon (TOC) Vs Irradiation time from photocatalytic degradation of RhB.

Table

Table 1. Band gaps and colours of microcrystalline $ZnSb_2O_6$ and nanocrystalline N - doped $ZnSb_2O_6$

O/F ratio	Band gap (eV)	Colour
2	2.82	Blue
1	2.90	Greenish Blue
0.5	3.20	Pale Yellow
Solid State	3.35	White

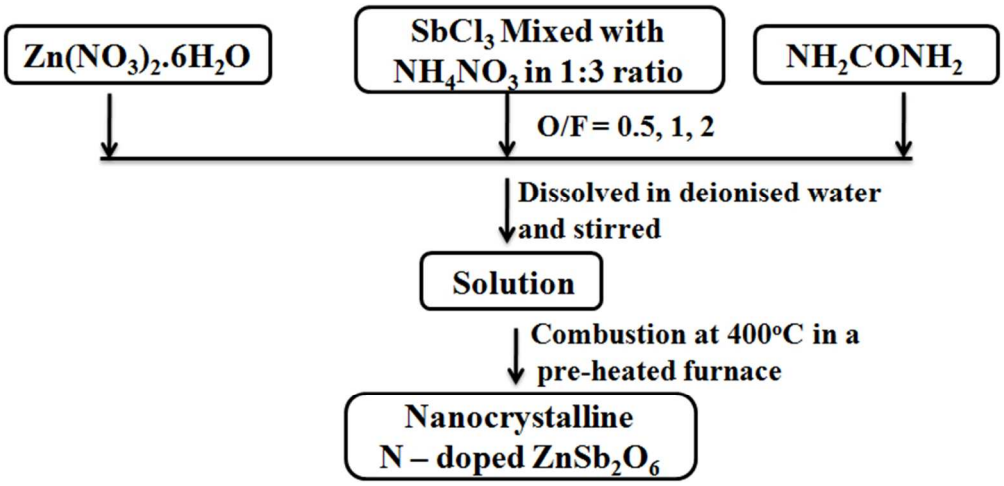

Figure 1

67x40mm (300 x 300 DPI)

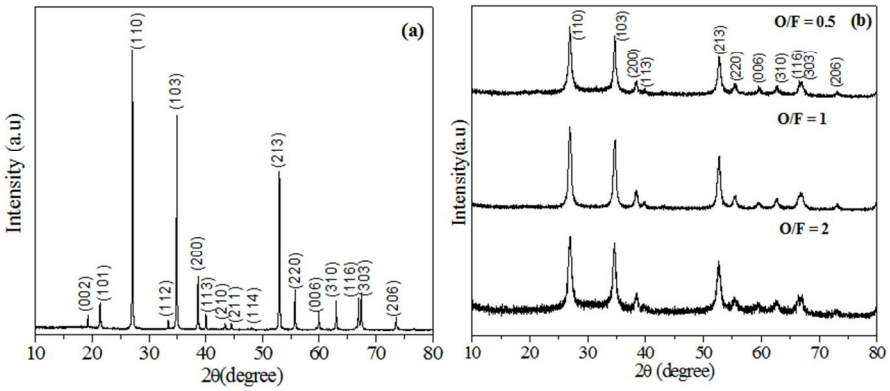

Figure 2

83x41mm (300 x 300 DPI)

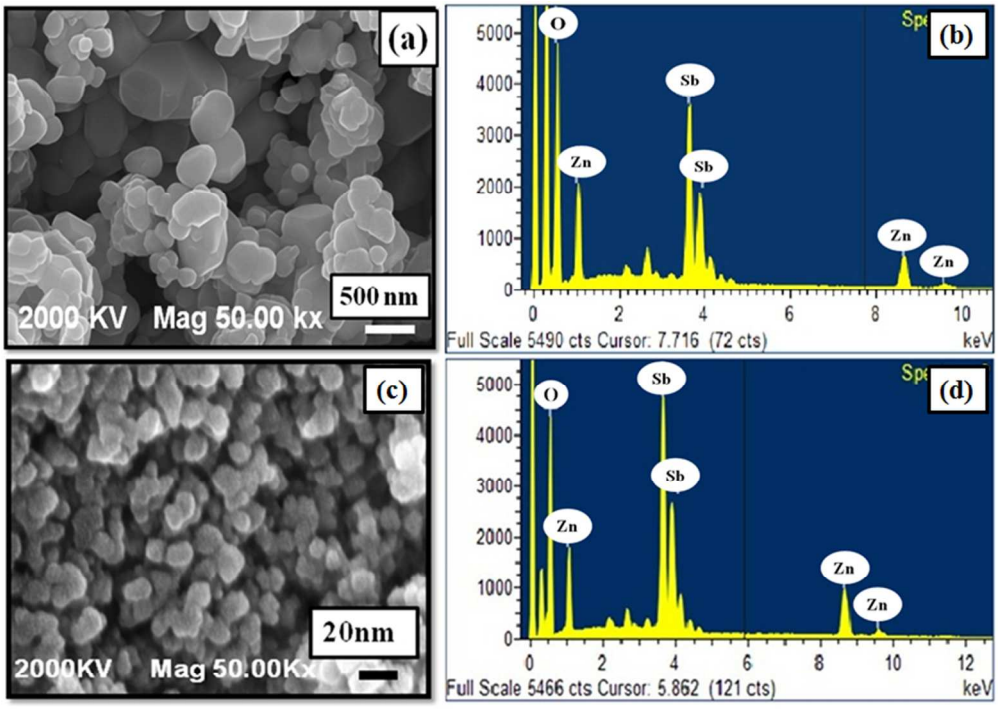

Figure 3

71x54mm (300 x 300 DPI)

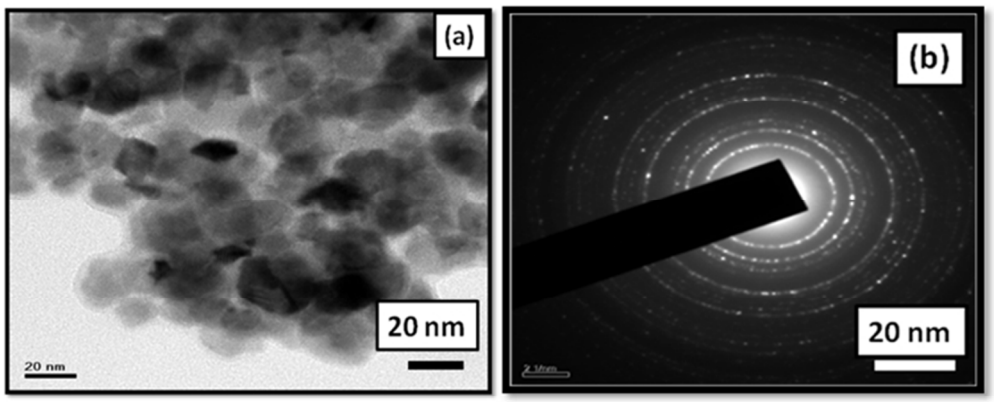

Figure 4

63x31mm (300 x 300 DPI)

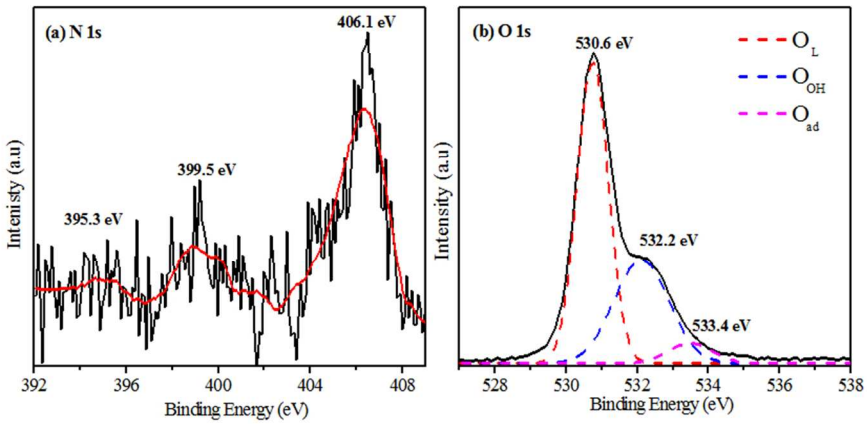

Figure 5

80x42mm (300 x 300 DPI)

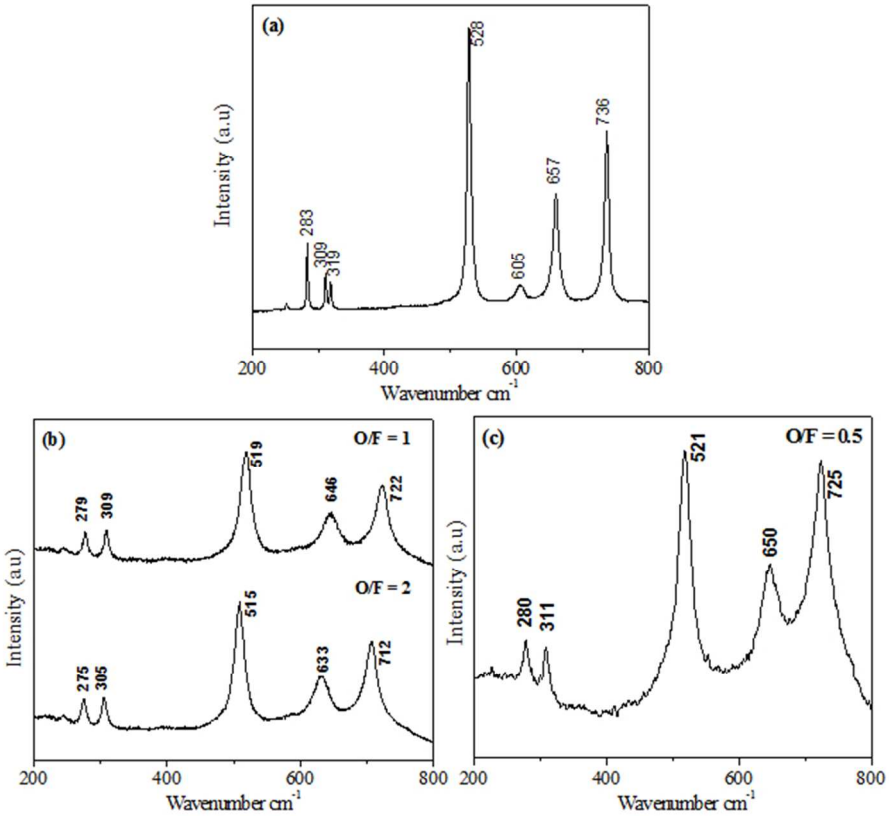

Figure 6

60x56mm (300 x 300 DPI)

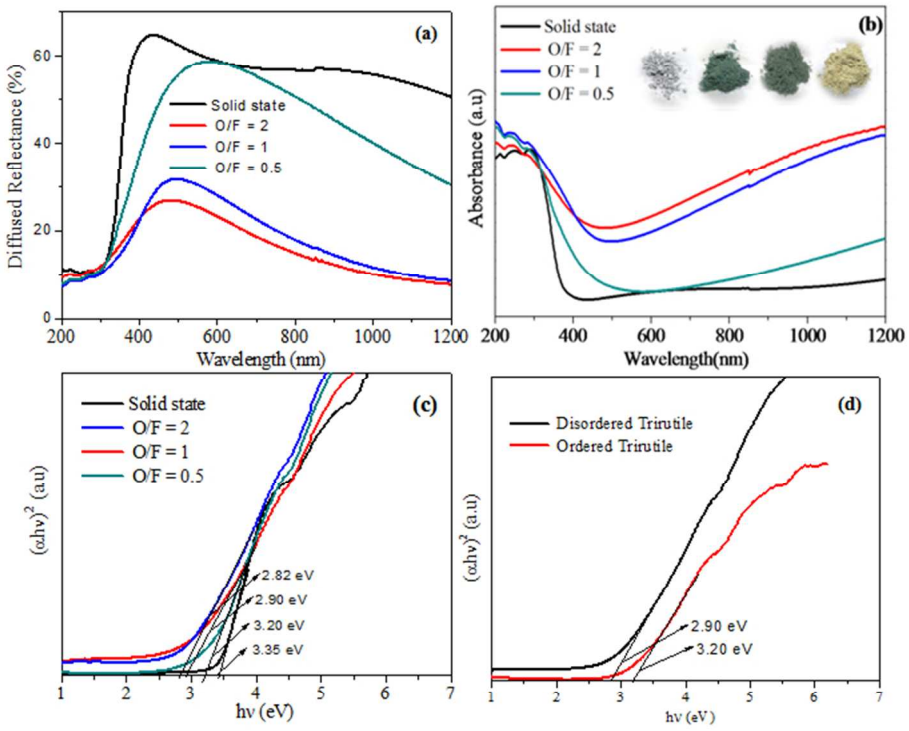

Figure 7

63x53mm (300 x 300 DPI)

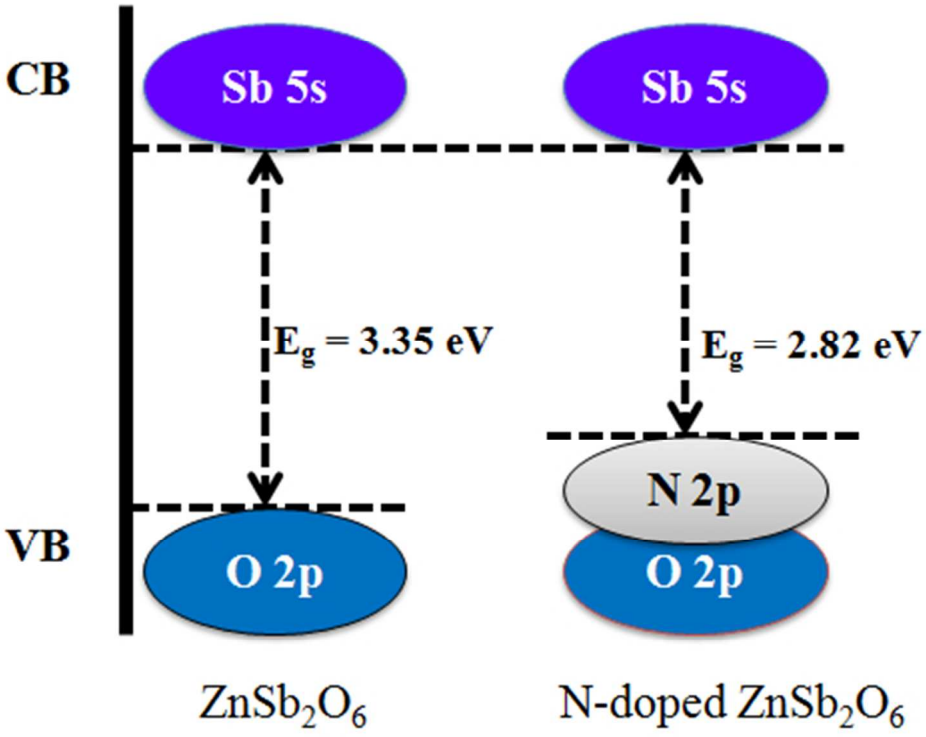

Figure 8

42x42mm (300 x 300 DPI)

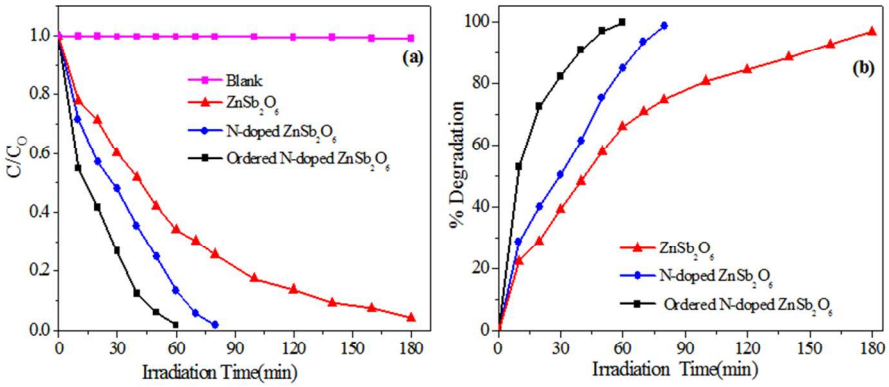

Figure 9

79x38mm (300 x 300 DPI)

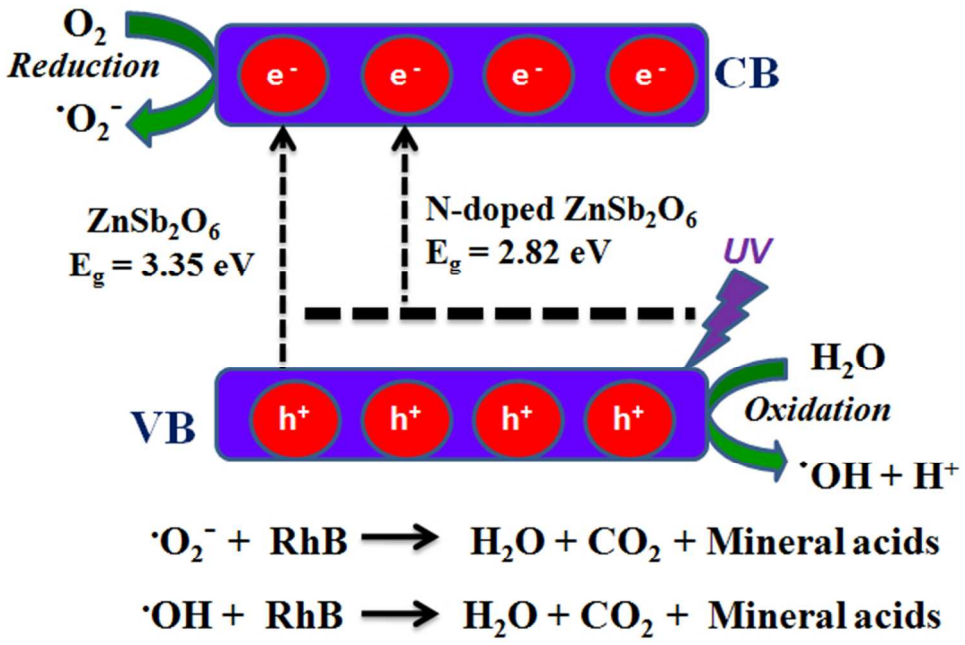

Figure 10

57x43mm (300 x 300 DPI)

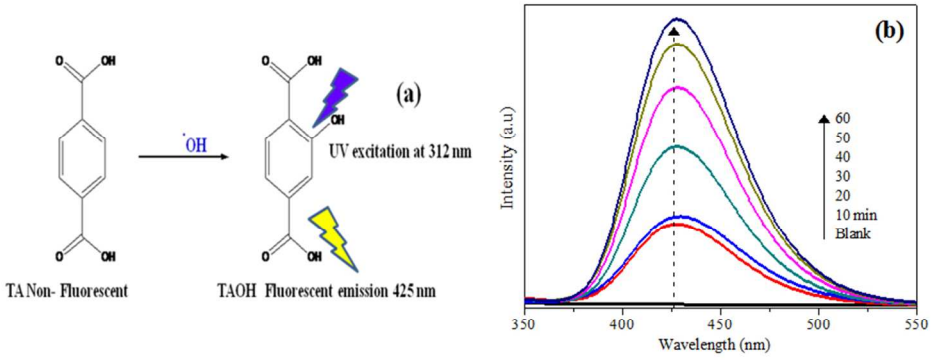

Figure 11

79x36mm (300 x 300 DPI)

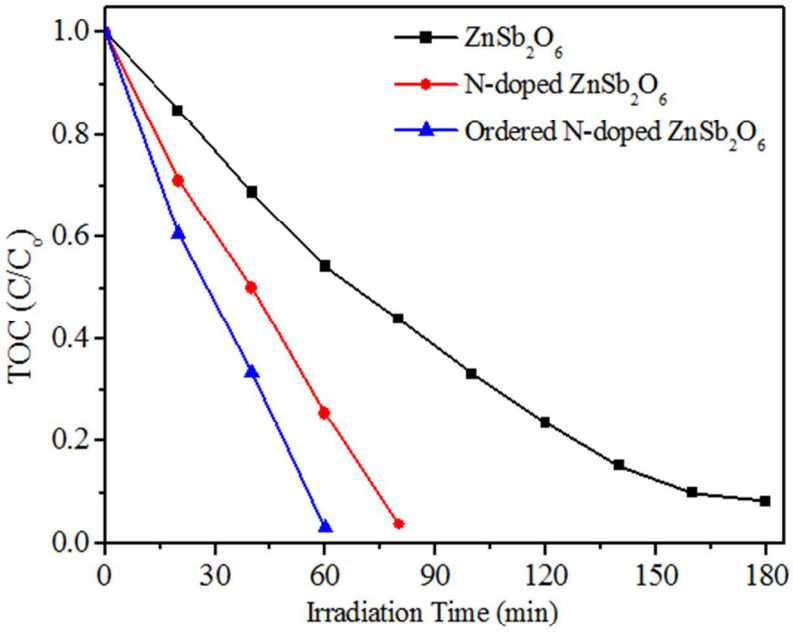

Figure 12

56x45mm (300 x 300 DPI)